Structural Engineering and Mechanics, *Vol. 65, No. 6 (2018) 771-784*
DOI: https://doi.org/10.12989/sem.2018.65.6.771

Stochastic responses of isolated bridge with triple concave friction pendulum bearing under spatially varying ground motion

Muhammet Yurdakul*[1] and Sevket Ates[2]

[1]*Department of Civil Engineering, Bayburt University, 69000, Bayburt, Turkey*
[2]*Department of Civil Engineering, Karadeniz Technical University, 61080, Trabzon, Turkey*

(Received September 8, 2017, Revised January 22, 2018, Accepted January 23, 2018)

Abstract. This study aims to investigate the stochastic response of isolated and non-isolated highway bridges subjected to spatially varying earthquake ground motion model. This model includes wave passage, incoherence and site response effects. The wave passage effect is examined by using various wave velocities. The incoherency effect is investigated by considering the Harichandran and Vanmarcke coherency model. The site response effect is considered by selecting homogeneous firm, medium and soft soil types where the bridge supports are constructed. The ground motion is described by power spectral density function and applied to each support point. Triple concave friction pendulum (TCFP) bearing which is more effective than other seismic isolation systems is used for seismic isolation. To implement seismic isolation procedure, TCFP bearing devices are placed at each of the support points of the deck. In the analysis, the bridge selected is a five-span featuring cast-in-place concrete box girder superstructure supported on reinforced concrete columns. Foundation supported highway bridge is regarded as three regions and compared its different situation in the stochastic analysis. The stochastic analyses results show that spatially varying ground motion has important effects on the stochastic response of the isolated and non-isolated bridges as long span structures.

Keywords: triple concave friction pendulum bearing; spatially varying earthquake ground motion; stochastic analysis; isolated bridge

1. Introduction

When a highway bridge as an important engineering structure collapses during earthquake, transportation is affected and introduces various hitches. These types of structure are constructed against severe earthquake ground motion. Thus, using stochastic approach considering incoherence, wave-passage and site-response effect along with seismic isolation system should use on designing long span structure as a highway bridge. Earthquake ground motion is described by power spectral density function as a random excitation in the stochastic analysis. Variation of ground motion is considered in the stochastic analysis. Incoherence, wave-passage and site-response effects should be considered in dynamic analysis of structural systems since the earth is inhomogeneity and complicated. The incoherence effect results from reflections and refractions of seismic waves through the soil during their propagation. The wave-passage effect results from the difference in the arrival times of waves at support points. The site-response effect is caused by differences the local soil conditions at the different support points.

Triple concave friction pendulum (TCFP) bearing is an innovative and viable isolation system using in new and need of strengthening bridges and other structures. This system based on one of the most effective sliding isolation system, namely friction pendulum system, is invented by Zayas *et al.* (1989). The TCFP bearing system consists of two facing concave stainless steel surfaces and an articulated slider is separately placed between the two spherical stainless-steel surfaces. Namely, in the later system motions occur in three sliding surfaces, so the system is named as triple. The principles of operation and force-displacement relationship of the TCFP bearing are developed by Fenz and Constantinou (2008a). There are some studies to indicate that the TCFP bearing system is more effective than the other sliding systems on severe earthquake ground motion (Barbas *et al.* 2011, Bucher 2011, Yurdakul *et al.* 2014, Tajammolian *et al.* 2014, Loghman and Khoshnoudian 2015, Fallahian *et al.* 2015). Bi-directionally series spring model is proposed by Fenz and Constantinou (2008b) to exactly model for typically designed TCFP bearing. The model compares well to experimental tests. This model is used to model TCFP bearing by some studies (Yurdakul and Ates 2011, Ates and Yurdakul 2011). Fadi and Constantinou (2009) described simplified methods of analysis structures isolated with the TCFP bearing. The method provides good and often conservative estimates of isolator displacement demands and isolator peek velocities. Morgan and Mahin (2012) propound that selecting the appropriate values for the friction coefficients and radii of curvature of the TCFP bearing is achieved different behavior under service, design and maximum considered excitation.

Long structures like bridges, dams and pipelines are significantly influenced by spatially varying ground motions. Dynamic response analysis long span non-isolated and isolated bridges subjected to spatially varying ground

∗Corresponding author, Ph.D.
E-mail: myurdakul@bayburt.edu.tr

http://www.techno-press.com/journals/sem&subpage=7
ISSN: 1225-4568 (Print), 1598-6217 (Online)

motions was examined by Harichandran and Wang (1988), Zerva (1991), Lou and Zerva (2005). Ates *et al.* (2005) studied on stochastic responses of non-isolated and seismically isolated highway bridge with single friction pendulum (SCFP) bearing under spatially ground earthquake motions. The study demonstrated that SCFP bearing system has important effects on stochastic responses of bridges to spatially varying ground motions. Ates *et al.* (2006) performed a study of spatially varying ground motions on stochastic response of isolated bridge with friction pendulum bearing systems. Analysis results pointed out that spatially varying ground motion should be taken account in the analysis to be factual in calculating isolated bridges. Ates *et al.* (2009) compared stochastic response of non-isolated and isolated cable-stayed bridge with double concave friction pendulum (DCFP) bearing subjected to spatially varying ground motion. The study pointed out that cable-stayed bridge with isolation system subjected to spatially varying ground motion significantly underestimates the deck and the tower responses. Wang *et al.* (2015) studied wave passage effect on seismic performance of a super-long-span suspension bridge. The study found out that seismic performance was influenced by variance of wave velocity. Apaydın *et al.* (2016) investigated structural responses of Fatih Sultan Mehmet Bridge under spatially varying ground motions. It is emphasized that spatially varying ground motion should be taken account in the extended structures like bridge. Adanur *et al.* (2016) performed an analysis of multiple support seismic response of Bosphorous Bridge for various random vibration methods. It is shown in the analysis results; structural responses substantially depend on frequency contents of power spectral density functions and intensity for a random excitation analysis.

Although stochastic responses of cable-stayed and highway bridges isolated with different sliding systems have been investigated, the TCFP bearing system exhibited more effective behavior than other sliding systems has not been widely investigated so far. The aim of this study is to compare the stochastic responses of the non-isolated and isolated highway bridges. The TCFP bearings are used to increase the earthquake resistance of the bridge subjected to the spatially varying earthquake ground motion which is considered the incoherency, wave passage and site response effects. For providing site response effects, different soil cases at the bridge supports are take into consideration.

2. Description of triple concave friction pendulum

TCFP bearing based on SCFP bearing was proposed by Zayas *et al.* (1989). Differences between TCFP bearing and conventional friction pendulum bearing are multiple changes in stiffness and strength with increasing amplitude of displacement (Fadi and Constantinou 2009). The TCFP bearing shown in Fig. 1 is consisted of two facing concave stainless steel surfaces coated with Teflon separated by a placed slider assembly. R_i is the radius of curvature of surface i, h_i is the radial distance between the pivot point and surface i, μ_i is the coefficient of friction at the sliding surface i and d_i is the displacement capacity of the surface i.

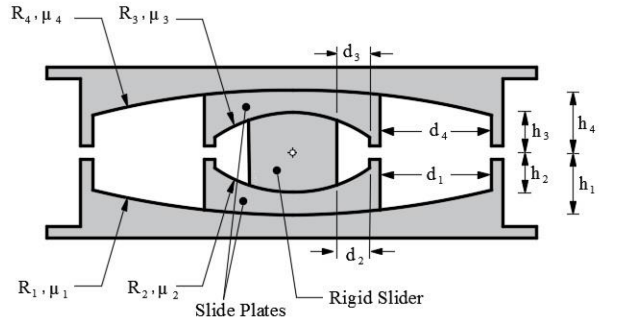

Fig. 1 The cross-section of the TCFP bearing and its definition of dimension

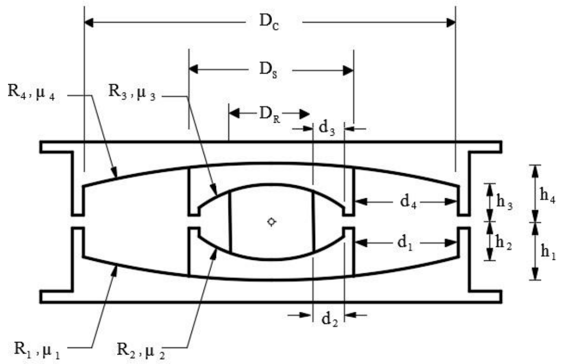

Fig. 2 Parameters of the TCFP bearing

Outer concave plates have effective radii $R_{eff\,1} = R_1 - h_1$ and $R_{eff4} = R_4 - h_4$. The articulated slider assembly consists of two concave plates separated by a rigid slider. While the innermost slider is rigid, the assembly has the capability to rotate to accommodate differential rotations of the top and bottom plates. The friction coefficients on these concave plates are μ_1 and μ_4. The inner concave plates have effective radii $R_{eff\,2} = R_2 - h_2$ and $R_{eff\,3} = R_3 - h_3$. Additionally, these surfaces are also coated with Teflon. The friction coefficients on these concave plates are μ_2 and μ_3. Unlike the SCFP and DCFP, in the TCFP bearing there is no mechanical constraint defining which defined location of pivot point (Fenz and Constantinou 2008a, b). In case economic benefits are considered, there is insignificant differentiation in the cost of the SCFP and the DCFP bearings of size. However, the TCFP bearing is cost effective as per bearing size and displacement capacity.

2.1 TCFP bearing design

2.1.1 Determination of geometric properties

The TCFP bearing has 16 parameters, of which 12 are geometry dependent. The other four parameters are composed of the friction coefficient. These parameters are very difficult to determine in optimization studies. The standard of bearing parameters and conformation used before is favorable about economic and stability. Therefore, it should be connected to producing company and claim the most appropriate forms of bearing. Then designer determines favorable bearing requested.

In this study, a sample design proposed by Constantinou *et al.* (2011) is used to determined parameters of TCFP bearing. The parameters are shown in Fig. 2 was studied to determine. In general, it is adjusted as R_1=R_4, R_2=R_3, d_1=d_4 and d_2=d_3.

In generally, diameter of concave plates, R_1 and R_2, are equal to 2235 mm and 3048 mm respectively. However, diameters of these surfaces are selected as 3092 mm because earthquake record is used analysis and piers are supported on different soil conditions. When the diameter is selected bigger value, re-centering force is not enough for a Design Basis Earthquake (DBE). This situation is checked by Eq. (1).

$$T \leq 28\left(\frac{0.05}{\mu}\right)^{\frac{1}{4}}\left(\frac{D}{g}\right)^{\frac{1}{2}} \tag{1}$$

Where μ is equal to the characteristic strength of TCFP bearing divided by the normal load supported isolation devices. D represents design displacement capacity. A preliminary estimation of diameter of concave plate, D_c, is selected to be 1778 mm (typically). Calculations based on simplified procedure indicated that this size of plate is enough. Diameter of concave plate could be selected bigger or smaller. Selected diameter could be changed depends on desirable friction of coefficient and axial load supported by bearing. In this study, TCFP bearing is designed according to axial loads which are W_1=9094 kN and W_2=12122 kN. Other concave plates, D_S and D_R, are selected to be 584 mm and 457 mm, respectively.

Heights of sliders (h_1+h_4, h_1+h_4) are selected as 406 mm and 305 mm, respectively. These values can be manufactured in different size discussed with consultation with manufacturers. They should not be calculated again because they do not affect behavior of bearing. Diameter of concave surfaces 1 and 2 are selected as 3962 mm and 1555 mm, respectively. The height of plates 1 and 2 are selected as 203 mm and 152 mm, respectively. The displacement capacity of i^{th} surface is determined by Eq. (2).

$$d_i^* = d_i \frac{R_{effi}}{R_i} \tag{2}$$

where d_i^* is actual displacement capacity of i^{th} surface, d_i is displacement capacity of i^{th} surface. The actual displacement capacity of surface 1 and 4 is calculated as 566 mm. The actual displacement capacity of surface 2 and 3 is calculated as 57 mm.

2.1.2 Determination of coefficient of friction

Bearing pressure is different on surfaces 1-4 and 2-3. Pressure of each of the surface is calculated by Eq. (3).

$$P = \frac{W}{\pi (D/2)^2} \tag{3}$$

in which P is bearing pressure, W is the vertical compressive load on the bearing and D is size of surface whose pressure is calculated. Tri-cycle coefficient of friction is determined by Eq. (4).

$$k_{3ccf} = 0.122\text{-}0.01\ P \tag{4}$$

Table 1 Properties of TCFP and Combined System

	W_1=9094 kN	W_2=12122 kN	Combined system (kN)
R_{eff1}=R_{eff4} (mm)	3759	3759	3759
R_{eff2}=R_{eff3} (mm)	1403	1403	1403
d_1^*=d_4^*(mm)	566	566	566
d_2^*=d_3^*(mm)	58	58	58
μ_1=μ_4 Lower bound	0.058	0.041	0.048
μ_2=μ_3 Lower bound	0.037	0.010	0.021
μ Lower bound	0.050	0.030	0.038
μ_1=μ_4 Upper bound	0.096	0.069	0.081
μ_2=μ_3 Upper bound	0.061	0.016	0.035
μ Upper bound	0.083	0.049	0.064

One-cycle coefficient of friction is determined by Eq. (5).

$$k_{1ccf} = 1.2 \times k_{lbcf} \tag{5}$$

where k_{lbcf} is lower bound coefficient of friction adjusted for high velocity. Upper bound coefficient of friction is determined by Eq. (6).

$$k_{ubcf} = \lambda_{max} \times k_{1ccf} \tag{6}$$

λmax results from aging, contamination and travel. It is selected as 1.386. The frictional properties of combined system are calculated by Eq. (7).

$$\mu_{ib} = \frac{2W_1\mu_{1i} + 2W_2\mu_{2i}}{2W_1 + 2W_2} \tag{7}$$

where μ_{ib} is coefficient of friction of i^{th} surface in the combined situation. μ_{1i} and μ_{2i} are coefficient of friction of i^{th} surface in case vertical load is W_1 and W_2, respectively. The properties of two different load cases are given in Table 1.

Effective coefficient of friction was determined by Ates and Constantinou (2011) for the DCFP bearing system. In the same way, effective coefficient of friction for the TCFP bearing is calculated by Eq. (8).

$$\mu_e = \frac{\mu_1(R_1\text{-}h_1) + \mu_2(R_2\text{-}h_2) + \mu_3(R_3\text{-}h_3) + \mu_4(R_4\text{-}h_4)}{R_1 + R_2 + R_3 + R_4 - h_1 - h_2 - h_3 - h_4} \tag{8}$$

Seismic device as the TCFP bearing has an important role to changing natural period of the supported structure. The natural period of the vibration is given by Eq. (9).

$$T = 2\pi\sqrt{\frac{R}{g}} \tag{9}$$

where R is the radius of spherical concave surface and g is the acceleration of gravity. Eq. (9) indicated that the natural period of vibration is independent of mass, but it is controlled by the radius of the concave surfaces. Therefore, it is too easy to change natural period of the supported structure. In addition, with the weight of the structure changing, the natural period of supported structure does not change. This natural period is period of the both isolated

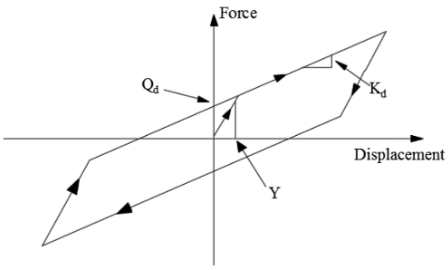

Fig. 3 Force-displacement relationship

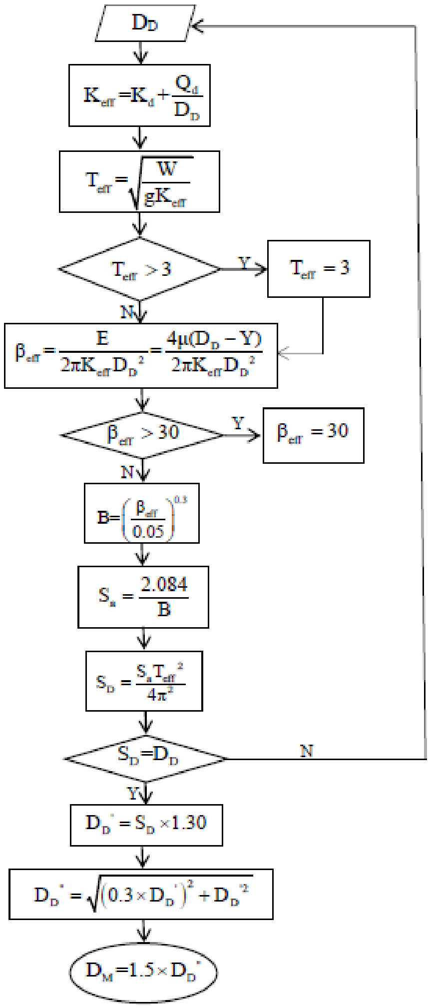

Fig. 4 Flow chart of single mode method

structure and the seismic isolation system. The isolated period begins to dominate when the friction force is exceeded. Period of the seismic isolated structure is equal to non-isolated structure when the earthquake force is small than friction force of the device. When the earthquake force exceeds frictional forces, dynamic responses are controlled by seismic isolation device. The force-displacement relationship of the Single Concave Friction Pendulum (SCFP) bearings in any direction may be given by the Eq. (10).

$$F = \frac{W}{R} v_b + \mu_s W \mathrm{Sign}(\dot{v}_b) \tag{10}$$

where W, R, v_b, μ_s, and $\dot{v}_b$ are the total weight carried by the SCFP, the radius of the spherical concave surface, the sliding displacement, the coefficient on the sliding surface and the sliding velocity, respectively. Sign is the signum function. The lateral restoring stiffness of the SCFP is given by the Eq. (11).

$$k_b = \frac{W}{R} \tag{11}$$

It is also shown in Eq. (11) that the stiffness of the pendulum depends on the weight carried by the bearing. Equivalent stiffness of the bearing is given by Eq. (12) (Scheller and Constantinou 1999).

$$k_{eş} = \frac{W}{R_{eff}} + \frac{\mu_e W}{(v_b)_{max}} \tag{12}$$

where $(v_b)_{max}$ is maximum displacement capacity of the SCFP, f_{min} is minimum mobilized coefficient of friction. The stiffness of the FPS system before it sliding is given by Eq. (13).

$$k_e = \frac{f_{min} W}{v_b} \tag{13}$$

where v_b is displacement of bearing.

2.1.3 Determination of displacement capacity of TCFP

The single mode method of analysis, spectrum analysis and time history analysis are used to determine displacement capacity of the TCFP bearing (Constantinou *et al.* 2011). The spectrum and the time history analyses are performed in SAP2000 (Computers and Structures Inc 2007). Results of these analyses are compared each other and displacement capacity of TCFP bearing is determined.

Single mode method of analysis is performed in the design earthquake (DE). Analyses procedure of seismic isolation system for upper bound by using bilinear hysteretic model is given below. The force-displacement relationship of isolation system is given Fig. 3. In this figure, K_d, Q_d and Y are represented post-elastic stiffness, characteristic strength and yield displacement, respectively. Post-elastic stiffness is given by Eq. (14).

$$K_d = \frac{W}{2R_{eff1}} \tag{14}$$

The post-elastic stiffness is calculated as 10441 kN/m by means of Eq. (14). The Characteristic strength is given by Eq. (15)

$$Q_d = \mu W \tag{15}$$

where μ is coefficient of friction of combined system. The characteristic strength is calculated as 2705 kN by means of Eq. (15). The yield displacement is given by Eq. (16).

$$Y = (\mu_1 - \mu_2) R_{eff2} \tag{16}$$

The yield displacement is calculated as 0,0634 m. by means of Eq. (16). Displacement of the TCFP bearing could be estimated at single mode analysis and shown in flow chart at Fig. 4.

1) The displacement capacity of TCFP bearing is selected as 0,278 m

2) The effective stiffness is given by Eq. (17) and calculated as 15375 kN/m.

$$K_{eff} = K_d + \frac{Q_d}{D_D} \tag{17}$$

3) The effective period is given by Eq. (18) and calculated as 3 s.

$$T_{eff} = \sqrt{\frac{W}{gK_{eff}}} \tag{18}$$

4) The effective damping is given by Eq. (19) and calculated as 0.311. But effective damping should be 0.3 to ensure re-centering of bearing at DE.

$$\beta_{eff} = \frac{E}{2\pi K_{eff} D_D^{\ 2}} = \frac{4\mu(D_D - Y)}{2\pi K_{eff} D_D^{\ 2}} \tag{19}$$

5) Damping reduction factor is given by Eq. (20) and calculated as 1.712.

$$B = \left(\frac{\beta_{eff}}{0.05}\right)^{0.3} \tag{20}$$

The spectral acceleration of response spectrum of PUL164 component of 1971 San Fernando earthquake for 5% damping is used. The corresponding value in the effective period in the response spectrum is 2.084 m/s^2. The design displacement is calculated as 0,272 m and given by Eq. (21)

$$S_D = \frac{S_a T_{eff}^{\ 2}}{4\pi^2 B} \tag{21}$$

In a similar way, the displacement of TCFP bearing was estimated using the bilinear hysteretic model of the isolated system according to the lower bound condition. Analyses results obtained by using single mode method of analysis for characteristics of the isolator used for the lower and upper bound conditions are given in Table 2.

The response spectrum analysis is performed using SAP2000 commercial software. Each isolator device is represented horizontal stiffness based on single mode method of analysis. To obtain a response spectrum according as a damping ratio differs from original response spectrum and Eq. (22) (ASCE 41-06 Eq. (1.13)) is used.

$$B = \frac{4}{5.6 - \ln(100\beta_{eff})} \tag{22}$$

Where β_{eff} is effective damping ratio, B is the coefficient that multiplies the 5% damped spectrum curve. The values, β_{eff} and T_{eff}, are used obtained from single mode method are used. β_{eff} is calculated as 28% and 30% for lower and upper bound, respectively. B is calculated as 1,759 and 1,819 for lower and upper bound, respectively. Changed spectrum ration is only used isolation mode. In other words, in periods greater than 0.8 T_{eff}, the ordinate of the 5% damped spectrum is reduced by B value. The reduced spectrum cure for lower and upper bound conditions are shown in Fig. 5. The displacement of the TCFP bearing obtained from analysis using response spectrum of PUL164 component of 1971 San Fernando earthquake for 5% damping is calculated as 314 mm.

Table 2 Displacement and damping capacities of the TCFP bearings using single mode method

Parameters	Design Earthquake (DE)		Maximum Considered Earthquake (MCE)	
	Lower bound	Upper bound	Lower bound	Upper bound
Displacement (mm)	284	278	578	565
Effective Damping	28%	30%	28%	30%

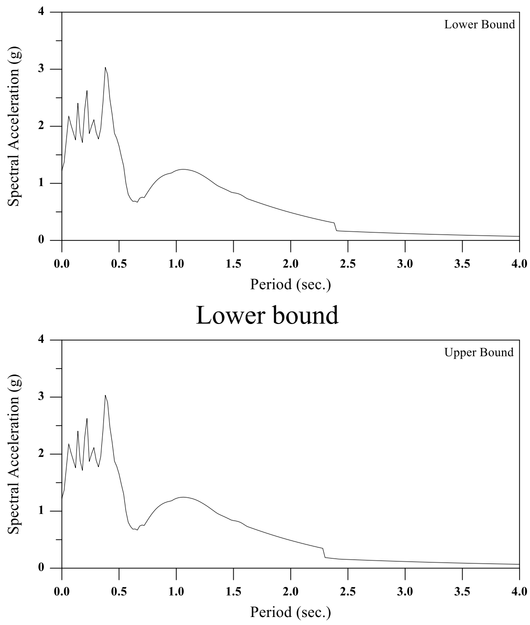

Lower bound

Upper bound

Fig. 5 Reduced response spectra

The nonlinear time history method is used for system stability control and evaluation of the performance of structural elements as well as for estimating the maximum displacement of the isolator. PUL164 component of 1971 San Fernando earthquake is used in time history analysis. Analyses results show that the maximum displacement of isolator reaches to 400 mm.

The results of single mode method of analysis, response spectrum and time history analysis are compared to determine displacement capacity of the TCFP bearing. The maximum displacement of the isolator is 578 mm. The dimensions of the isolator are suitable because the value is smaller than the maximum displacement capacity of the selected isolator.

3. Stochastic response

The variance of the i th total response is given by Eq.

(23)

$$\sigma^2_{z_i} = \sigma^2_{z_i^{qs}} + \sigma^2_{z_i^{d}} + 2\mathrm{Cov}(z_i^{qs},\ z_i^{d}) \quad (23)$$

Where $\sigma^2_{z_i^{d}}$ is the variance of the i th quasi-static response component, $\sigma^2_{z_i^{d}}$ is the variance of the i th dynamic response component and $\mathrm{Cov}(z_i^{qs},\ z_i^{d})$ is the covariance between the i th quasi-static and dynamic components. The variance of the i th quasi-static component can be written as Eq. (24).

$$\sigma^2_{z_i^{qs}} = \int_{-\infty}^{\infty} S^{qs}_{z_i}(\omega)d\omega = \sum_{l=1}^{r}\sum_{m=1}^{r} A_{il}A_{im}\int_{-\infty}^{\infty}\frac{1}{\omega^4} S_{\ddot{v}_{g_l}\ddot{v}_{g_m}}(\omega)d\omega \quad (24)$$

Where $S^{qs}_{z_i}(\omega)$ is the i th quasi-static component of the spectral density function of the structural response, r is the number of restrained degrees of freedom, $S_{\ddot{v}_{g_l}\ddot{v}_{g_m}}(\omega)$ is the cross-spectral density function of accelerations between supports l and m, A_{il} and A_{im} are equal to static displacements for unit displacements appointed to each support. The variance of the i th dynamic response component may be given in Eq. (25).

$$\sigma^{2d}_{z_i} = \int_{-\infty}^{\infty} S^{d}_{z_i}(\omega)d\omega = \sum_{j=1}^{n}\sum_{k=1}^{n}\sum_{l=1}^{r}\sum_{m=1}^{r}\psi_{ij}\psi_{ik}\Gamma_{lj}\Gamma_{mk}\int_{-\infty}^{\infty} H_j(-\omega)H_k(\omega)\, S_{\ddot{v}_{g_l}\ddot{v}_{g_m}}(\omega)d\omega \quad (25)$$

Where, $S^{d}_{z_i}$ is the i th dynamic component of the spectral density function of the structural response, n is the number of degrees of freedom, ψ is the eigenvectors, Γ is the modal participation factor and $H(\omega)$ is the frequency response function.

The mean of maximum value and its standard deviation are most important parameters in stochastic analysis. The maximum value can be given in Eq. (26) (Button *et al.* 1981, Dumanoğlu and Severn 1990).

$$\mu = p\sigma_Z \quad (26)$$

The standard deviation of the mean of the maximum value is given in Eq. (27) (Button 1981, Der Kiureghian 1980).

$$\sigma = q\sigma_Z \quad (27)$$

Where q and p are peak factors which are zero-crossing rate and functions of the time of the motion, respectively (Der Kiureghian and Neuenhofer 1991).

4. Spatially varying earthquake ground motion

Due to the complex nature of the earth, earthquake ground motion may not show the same behavior at each support point of long span structures such as bridge. This occurs by considering that travelling with finite velocity, coherency loss due to reflections-refractions and difference of local soil conditions at the supports. This variation gives rise to internal forces because of quasi-static displacement. In normally, quasi-static displacements do not produce internal force in the case of uniform ground motion.

Therefore, spatially varying ground motion should be considered while analyzing large structures. Spatially varying earthquake ground motion model includes incoherency, wave passage and site response effect. The incoherency effect results from reflections and refractions of seismic waves through to the soil during their propagation. The wave passage effect results from differences in the arrival times of waves at support points. The site response effect results from differences in local soil conditions at the support point. These effects are characterized by the coherency function in the frequency domain.

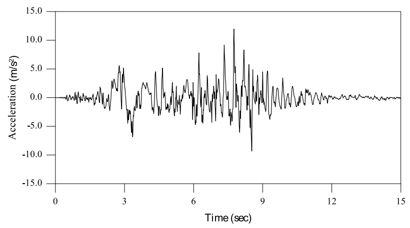

PUL164 component of Pacoima Dam record of 1971 San Fernando earthquake

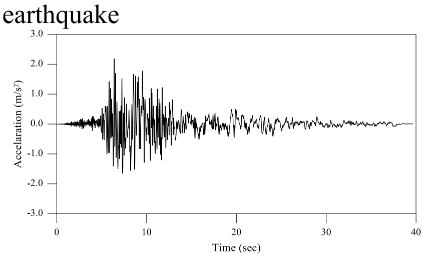

H-E03230 component of El Centro Array #3 record of 1979 Imperial Valley-06 earthquake

Fig. 6 Earthquake records used variance of the ground acceleration

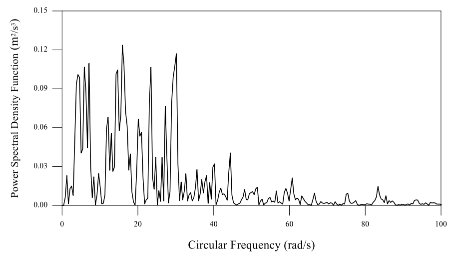

PUL164 component of Pacoima Dam record of 1971 San Fernando earthquake

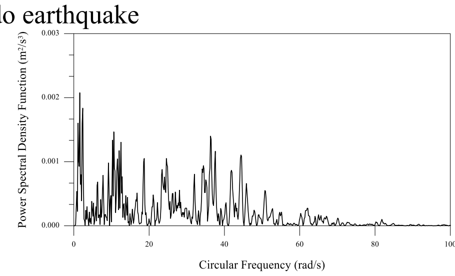

H-E03230 component of El Centro Array #3 record of 1979 Imperial Valley-06 earthquake

Fig. 7 Power spectral density function

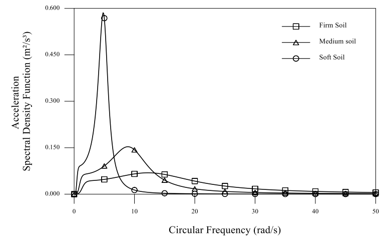

PUL164 component of Pacoima Dam record of 1971 San Fernando earthquake

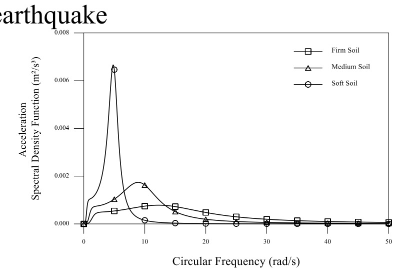

H-E03230 component of El Centro Array #3 record of 1979 Imperial Valley-06 earthquake

Fig. 8 Acceleration spectral density function

Table 3 Filter parameter of filtered white-noise process for different soil types

Soil Type	ω_f (rad/sec)	ξ_f	ω_g (rad/sec)	ξ_g
Firm	15.0	0.6	1.5	0.6
Medium	10.0	0.4	1.0	0.6
Soft	5.0	0.2	0.5	0.6

Table 4 Intensity parameter of filtered white-noise process for different soil types

Soil Type	S_0 (m^2/s^3)	
	San Fernando	Imperial Valley
Firm	0.037373	0.000425
Medium	0.055534	0.000631
Soft	0.077968	0.000887

In the stochastic analysis, the cross spectral density function of the earthquake ground motion, between support points *l* and *m* is given by Eq. (28) (Der Kiureghian and Neuenhofer 1991).

$$S_{\ddot{v}g_l \ddot{v}g_m}(\omega) = \gamma_{lm}(\omega)\sqrt{S_{\ddot{v}g_l \ddot{v}g_l}(\omega)\, S_{\ddot{v}g_m \ddot{v}g_m}(\omega)} \tag{28}$$

Where $\gamma_{lm}(\omega)$ is coherency function. The power spectral density function is suggested by Clough and Penzien (1993) given by Eq. (29).

$$S_{\ddot{v}g}(\omega) = S_0 \frac{\omega^4 + 4\xi_f^2\,\omega_f^2\,\omega^2}{\left(\omega_f^2-\omega^2\right)^2 + 4\xi_f^2\,\omega_f^2\,\omega^2}\;\frac{\omega^4}{\left(\omega_g^2-\omega^2\right)^2 + 4\xi_g^2\,\omega_g^2\,\omega^2} \tag{29}$$

Where S_0 is value of spectral density function of the white-noise process, first term and second terms are frequency responses of first and second filters depicting characteristics of the layers of soil medium above the rock bed. ω_f and ξ_f are the resonant frequency and damping of the first filter, ω_g and ξ_g are those quantities of the second filter.

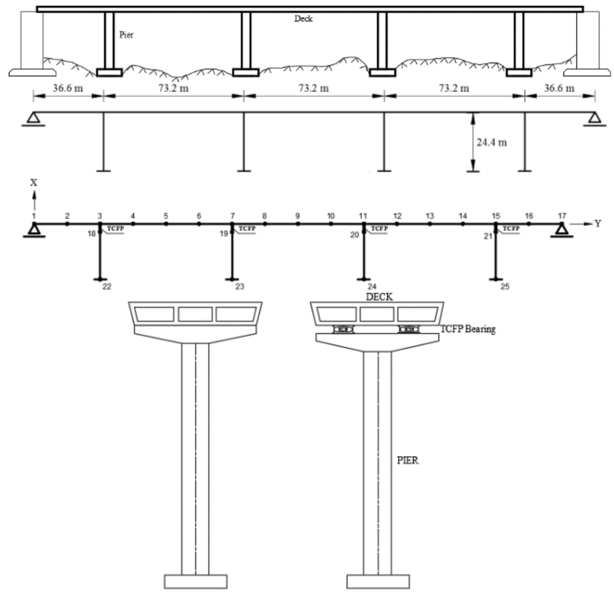

Fig. 9 Selected highway bridge model and its two-dimensional analytical model

Table 5 Properties of the bridge

Properties	Deck	Pier
Young's modules (MPa)	32000	32000
Cross section (m^2)	6,90	4,90
Moment of inertia in the case of vertical bending (m^4)	4,20	1,92
Moment of inertia in the case of lateral bending (m^4)	79,18	1,92
Torsional moment	14,18	3,84
Poisson's ratio	0,25	0,25
Unit weight (kN/m^3)	25,00	25,00
Unit length weight (kN/m)	165,60	122,75

In this study, S_o is obtained for each soil type equating the variance of the ground acceleration to the variance of the two earthquake records. These are PUL164 component of the San Fernando earthquake recorded at Pacoima dam in 1971 for firm soil and El Centro Array #3 component of the Imperial Valley-06 in 1979 for soft soil (Fig. 6). Their power spectral density function and their acceleration spectral density function for different soil types are given in Figs. 7-8. Soft, medium and firm soil types are used for the isolated and non-isolated bridge supports and the filter parameters for these soil types proposed by Der Kiureghian and Neuenhofer (1991) are also used as given Table 3. The calculated values of the intensity parameter for each soil type are given in Table 4.

The coherency function is proposed by Nakamura *et al.* (1993) and given by Eq. (30).

$$\gamma_{lm}(\omega) = \left|\gamma_{lm}(\omega)\right|^{i}\,\gamma_{lm}(\omega)^{w}\,\gamma_{lm}(\omega)^{s} \tag{30}$$

Where $\left|\gamma_{lm}(\omega)\right|^{i}$ indicates the incoherence effect,

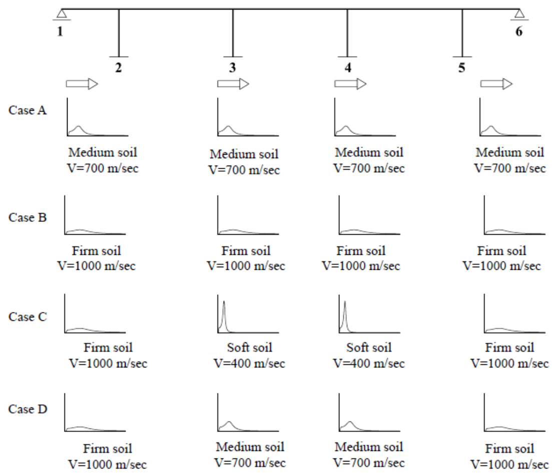

Fig. 10 Bridge subjected to spatially varying ground motions for different soil condition sets

Table 6 Periods of the bridges

Mode Number	Non-isolated (sec)		Isolated (sec)		
			TCFP		SCFP Ates *et al.* (2005)
	SVEM	SAP2000	SVEM	SAP2000	SVEM
1	1,1929	1,2279	3,6607	3,7473	2,8494
2	0,8144	0,8516	1,0310	1,0700	1,0241
3	0,6844	0,7197	0,7700	0,8090	0,7679
4	0,5784	0,6124	0,5964	0,6354	0,5964
5	0,2739	0,2959	0,3028	0,5914	0,3017
6	0,262	0,2842	0,2799	0,5900	0,2787
7	0,2354	0,2582	0,2419	0,5665	0,2411
8	0,2136	0,2368	0,2123	0,5645	0,2118
9	0,205	0,2283	0,2003	0,3235	0,2001
10	0,1698	0,1731	0,1718	0,3026	0,1717
11	0,1357	0,1566	0,1378	0,2672	0,1378
12	0,1301	0,1512	0,1297	0,2398	0,1297
13	0,1258	0,147	0,1239	0,2291	0,1239
14	0,0862	0,0878	0,0866	0,1653	0,0865
15	0,0583	0,0593	0,0585	0,1592	0,0584

$\gamma_{lm}(\omega)^w$ represents the complex valued wave-passage effect and $\gamma_{lm}(\omega)^s$ characterizes the complex valued site-response effect. The incoherency effect is proposed by Harichandran and Vanmarcke (1986) and given by Eq. (31).

$$\left|\gamma_{lm}(\omega)\right|^{i} = A\exp\left[-\frac{2d_{lm}}{\alpha\,\theta(\omega)}(1-A+\alpha A)\right] + (1-A)\exp\left[-\frac{2d_{lm}}{\theta(\omega)}(1-A+\alpha A)\right] \quad (31)$$

Where d_{lm} is distance between support points l and m; A, α, k, f_o and b are 0.636, 0.0186, 31200, 1.51 Hz and 2.95, respectively (Harichandran *et al.* 1996).

The wave-passage effect is given by Eq. (32) (Zerva 1991, Soyluk and Dumanoğlu 2004).

$$\gamma_{lm}(\omega)^{W} = \exp^{i(-\omega d^{L}_{lm}/v_{app})} \quad (32)$$

Mode 1: 3,7473 sec (longitudinal) Modal Participating Mass Ratio: 94,88%

Mode 2: 0,8090 sec (vertical) Modal Participating Mass Ratio: 40,79%

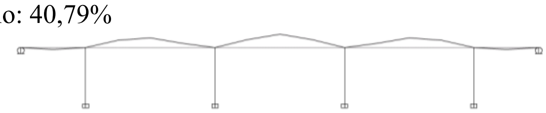

Mode 3: 0,6354 sec (vertical) Modal Participating Mass Ratio: 24,77%

Mode 4: 1,0705 sec (vertical) Modal Participating Mass Ratio: 19,53%

Mode 5: 0,5914 sec (longitudinal) Modal Participating Mass Ratio: 12,22%

Fig. 11 The first 5 mode shapes of the isolated bridge with the TCFP bearings

Mode 1: 1,2279 sec (longitudinal) Modal Participating Mass Ratio: 99,18%

Mode 2: 0,8516 sec (vertical) Modal Participating Mass Ratio: 42,99%

Mode 3: 0,7197 sec (vertical) Modal Participating Mass Ratio: 9,93%

Mode 4: 0,6124 sec (vertical) Modal Participating Mass Ratio: 6,16%

Mode 5: 0,2959 sec (vertical) Modal Participating Mass Ratio: 4,73%

Fig. 12 The first 5 mode shapes of the non-isolated bridge

Where v_{app} is the visible wave velocity. d^{L}_{lm} is projection of d_{lm} on the ground surface along the direction of propagation of seismic waves. The visible velocities used in

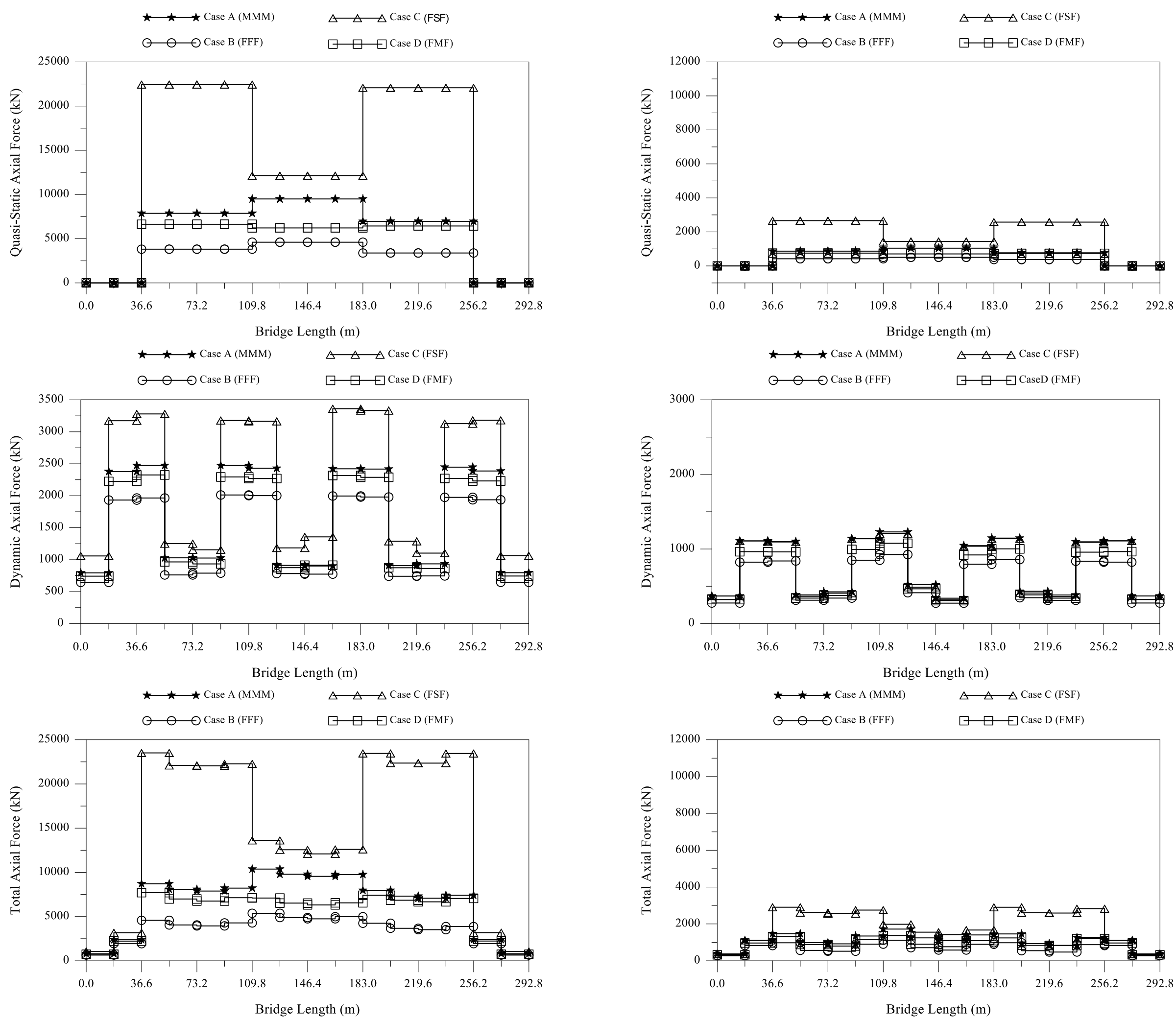

(a) Non-isolated (b) Isolated

Fig. 13 Mean of maximum axial forces of the non-isolated and isolated bridge decks

this study are selected as 400, 700, 1000 m/sec for soft, medium and firm soil, respectively.

The site response effect is given by Eq. (33) (Zerva 1991, Soyluk and Dumanoğlu 2004).

$$\gamma_{lm}(\omega)^{z} = \exp^{i\theta_{lm}(\omega)^{z}} \tag{33}$$

5. Numerical examples

A two-dimensional analytical model used by Ates *et al.* (2005) is selected as a numerical example to investigate the stochastic response of non-isolated and isolated bridge with the TCFP bearing. The selected highway bridge and its analytical model are shown in Fig. 9. The properties of the bridge are given in Table 5. Properties of the TCFP bearing employed in this study are given Table 6. Stochastic analyses of non-isolated and isolated bridge with the TCFP are performed for spatially varying earthquake ground motion by considered the incoherency, wave passage and site response effects.

For this purpose, four different soil situation sets are considered namely Cases A to D for the bridge supports and shown in Fig. 10.

Case A: All supports are assumed to be founded on medium soil type (Fig. 10). The soil condition where the structure is supported is defined as homogeneous. Incoherency effect and wave passage effect are considered

$$(\gamma_{lm}(\omega)^{d} \neq 1,\ \left|\gamma_{lm}(\omega)\right|^{k} \neq 1,\ \gamma_{lm}(\omega)^{z} = 1).$$

Case B: All supports are assumed to be founded on firm soil type (Fig. 10). The soil condition where the structure is supported is defined as homogeneous. Incoherency effect and wave passage effect are considered

$$(\gamma_{lm}(\omega)^{d} \neq 1,\ \left|\gamma_{lm}(\omega)\right|^{k} \neq 1,\ \gamma_{lm}(\omega)^{z} = 1).$$

Case C: While the side supports (1,2,5 and 6 in Fig. 10) are assumed to be founded of firm soil, the middle supports (3 and 4 in Fig. 10) are assumed to be founded on soft soil. In this case the incoherency, wave passage and site response effects are considered

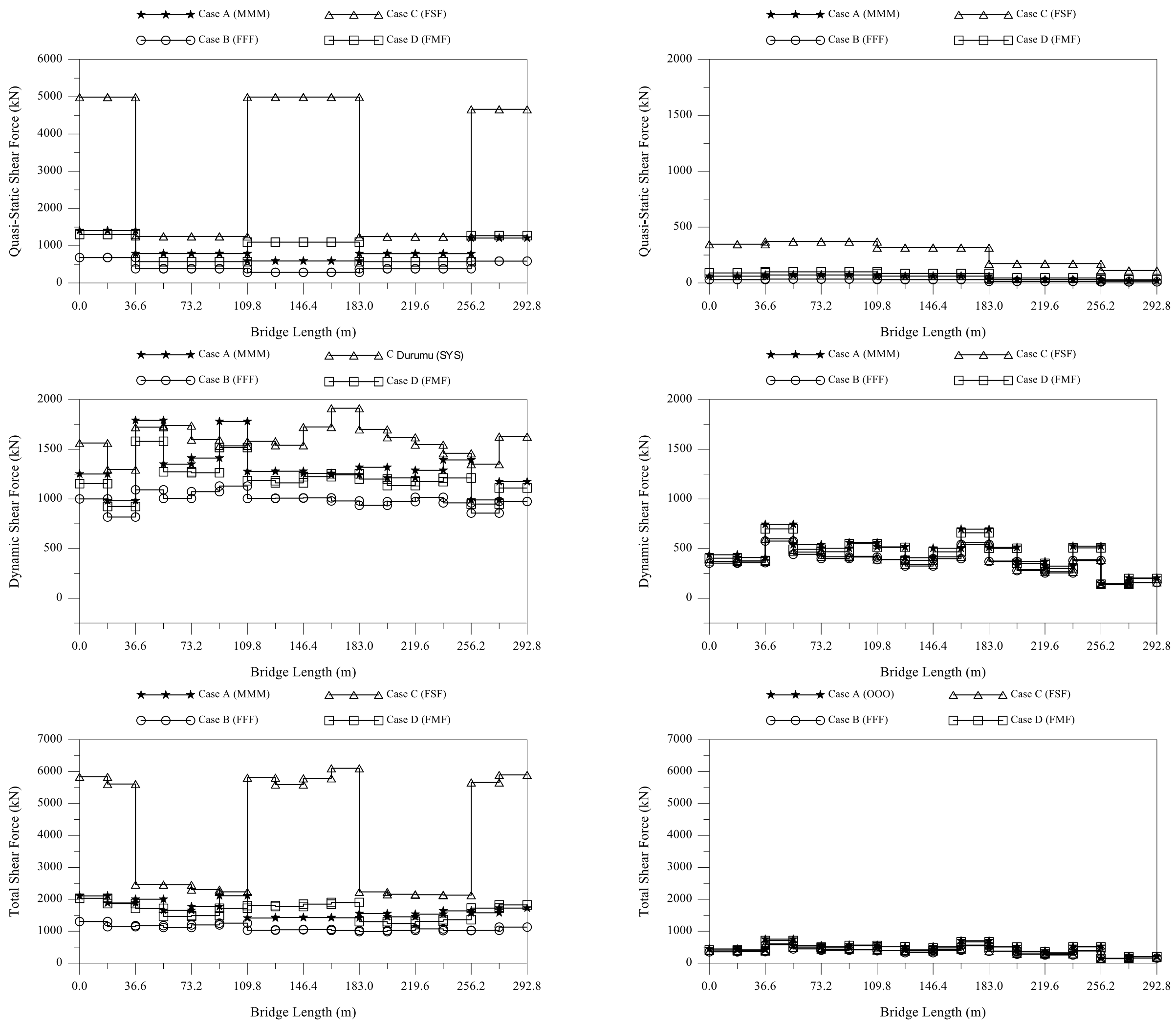

(a) Non-isolated (b) Isolated

Fig. 14 Mean of maximum shear forces of the non-isolated and isolated bridge decks

$$(\gamma_{lm}(\omega)^{d} \neq 1, \ \left|\gamma_{lm}(\omega)\right|^{k} \neq 1, \ \gamma_{lm}(\omega)^{z} \neq 1).$$

Case D: while the side supports (1, 2, 5 and 6 in Fig. 10) are assumed to be founded of firm soil, the middle supports (3 and 4 in Fig. 10) are assumed to be founded on medium soil. In this case the incoherency, wave passage and site response effects are considered

$$(\gamma_{lm}(\omega)^{d} \neq 1, \ \left|\gamma_{lm}(\omega)\right|^{k} \neq 1, \ \gamma_{lm}(\omega)^{z} \neq 1).$$

The bridge model subjected to spatially varying ground motions in the horizontal direction is shown in Fig 10. The horizontal input data is supposed to travel across the bridge from left to right side with finite velocities of 400, 700 and 1000 m/s for soft, medium and firm soil, respectively.

The stochastic analysis of spatially varying ground motion includes incoherency, wave passage and site response effects are performed with computer code SVEM (Dumanoglu and Soyluk 2002). However, computer code program called SVEM has not been performed a stochastic analysis of spatially varying ground motion of an isolated structure with the TCFP by now. Ates *et al.* (2005) carried out a stochastic analysis an isolated structure with the SCFP bearing. Considering the change components of the earthquake motion, behavior of the TCFP bearing is attached in the program and stochastic analysis of spatially varying ground motion includes incoherency, wave passage and site response effects are performed.

6. Numerical results

Stochastic analyses of non-isolated and isolated highway bridge with TCFP are performed for spatially varying ground motions by assuming that the different cases in this study. Four cases sets are considered in Fig. 10. The non-isolated and isolated highway bridge model subjected to spatially varying ground motions in the horizontal direction. This horizontal input is assumed to travel with finite velocities of 400, 700 and 1000 m/s.

Since bridges exhibit different behaviors, it is necessary to consider a larger number of modes compared to other structures (Dumanoglu and Severn 1987). Thus, the first 15 modes are selected according to modal participating mass ratio. Structures have the tendency to vibrate at certain

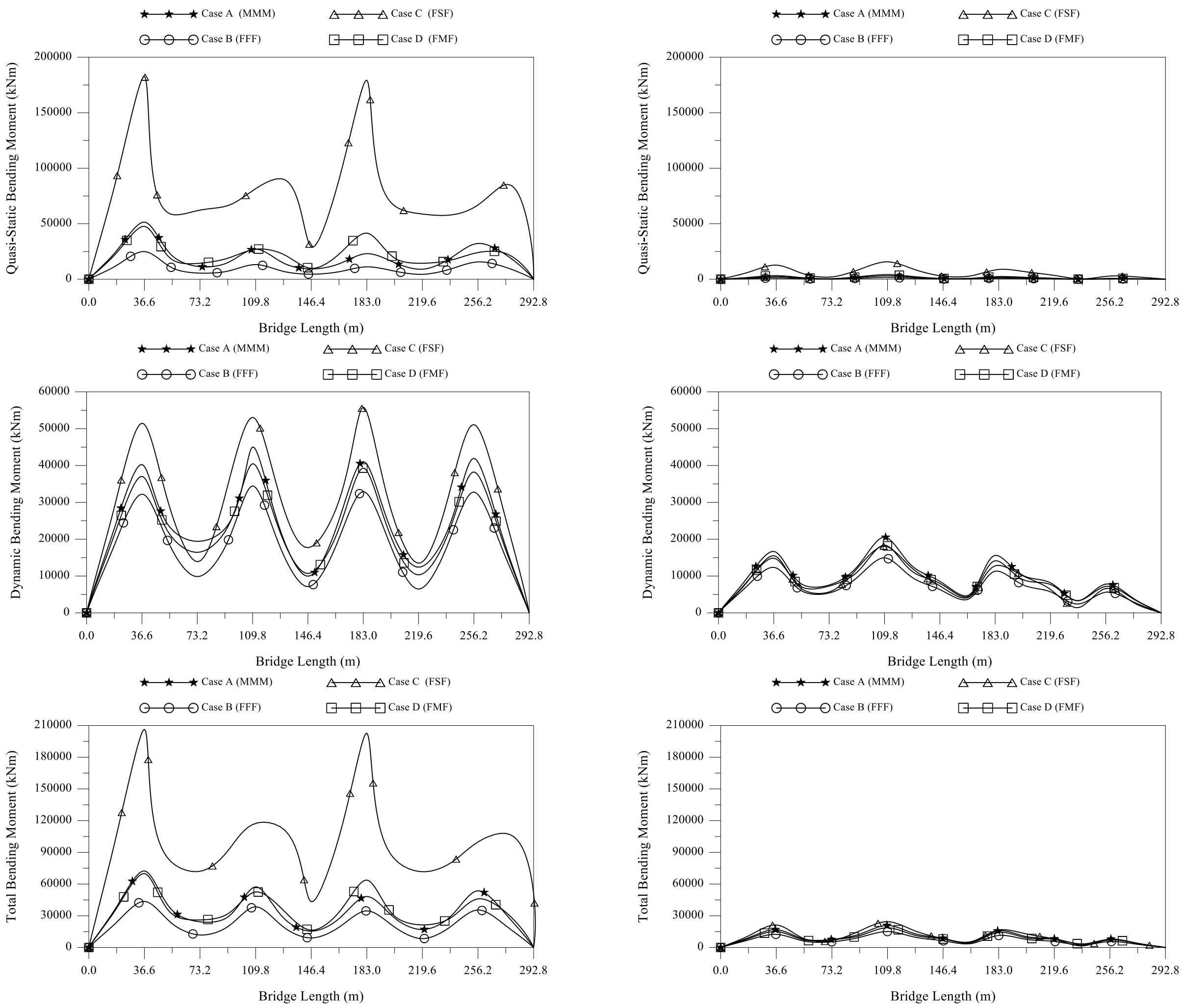

(a) Non-isolated (b) Isolated

Fig. 15 Mean of maximum bending moments of the non-isolated and isolated bridge decks

frequencies which are called natural frequencies that is associated with a mode shape that the model tends to assume when vibrating at that frequency.

When a structure is properly excited by a dynamic load with a frequency that coincides with one of its natural frequencies, the structure undergoes large displacements and stresses. This phenomenon is known as resonance.

The parameter is modal participating mass ratio (MPMR) in the selection of the mode number. Basically, the MPMR provides a measure of the energy contained within each resonant mode since it represents the amount of system mass participating in a particular mode. For a particular structure, with a mass matrix $[M]$, normalized mode shapes $[\Phi_i]$ and a ground motion influence coefficient $\{r\}$, participation of each mode can be obtained as the modal mass participation ratio is given by

$$\Gamma_i = \frac{[\Phi]_i^T [M]\{r\}}{[\Phi]_i^T [M][\Phi]_i^2} \tag{34}$$

Therefore, m mode with a large effective mass is usually a significant contributor to the response of the system. It is possible to calculate the MPMR for a particular direction (x, y or z). The sum of the effective masses for all modes in each response direction must equal the total mass of the structure. Priestley *et al*. (1996), among other authors, confirm that a sum of all MPMR, known as Cumulative Modal Mass Participation Ratio (CMPMR) of 80% to 90% in any given response direction can be considered sufficient to capture the dominant dynamic response of the structure,

$$80 \le \left(100 \cdot \sum_{i=1}^{n} \Gamma_i\right) \le 90 \tag{35}$$

where n is the number of modes taken under consideration. Therefore, if for example it is expected a vibration in the x direction, it can need to keep calculating modes until the sum of all MPMR in the x direction is about 80-90%. This should ensure a consistency in the results since it can compare the exciting frequency with the sufficient natural frequencies. It is seen that the sum of the MPMR for each direction is higher than 80%.

The two-dimensional analytical model of the isolated and non-isolated bridges are modeled and analyzed in SVEM (Dumanoglu and Soyluk 2002). The first 5 mode shapes obtained from the analysis is given in Figs. 11 and 12.

In addition, the isolated bridge with the TCFP bearing is

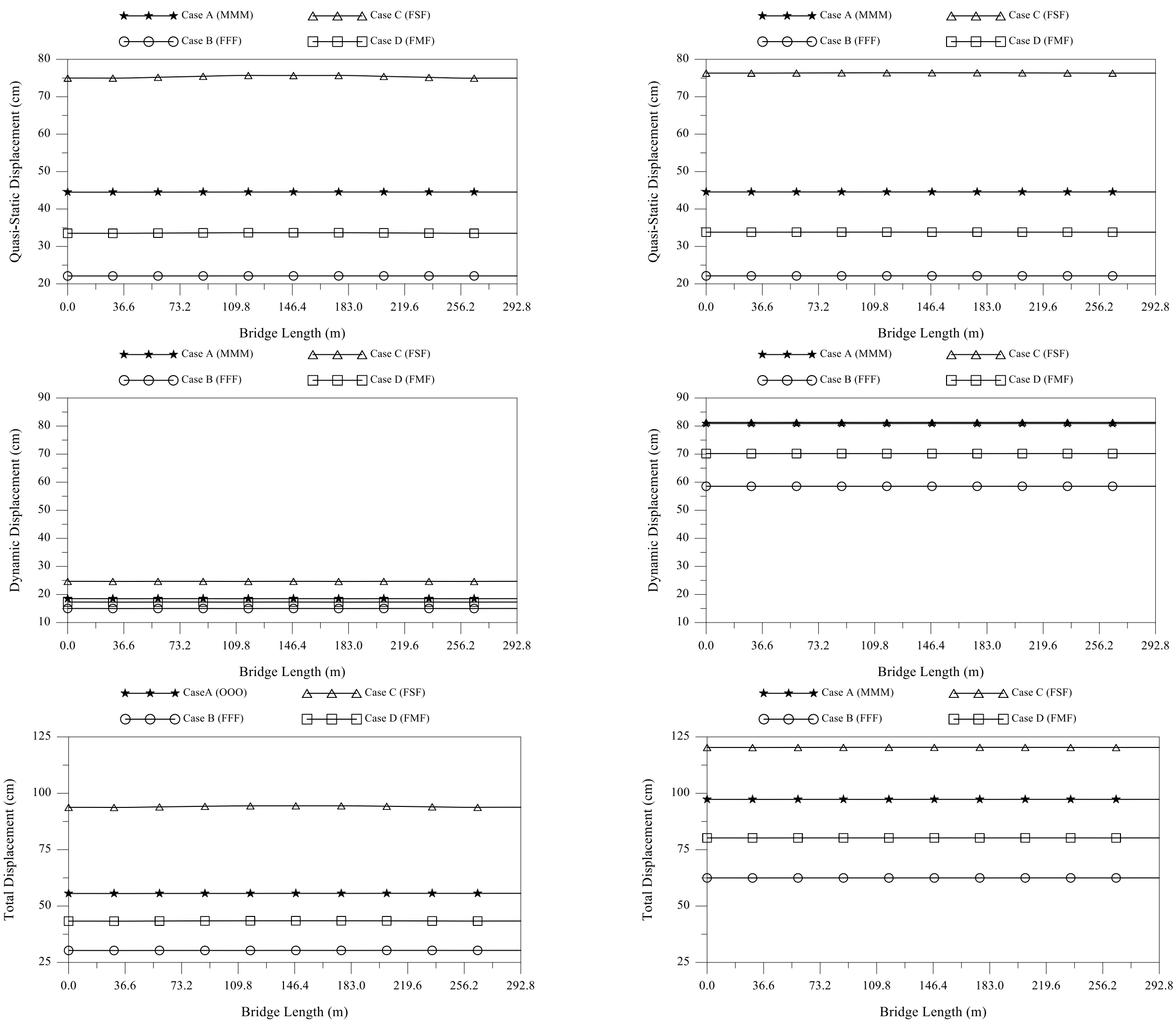

(a) Non-isolated (b) Isolated

Fig. 16 Mean of maximum horizontal displacements of the non-isolated and isolated bridge decks

modeled and analyzed in SAP2000 (Computers and Structures 2007). In Table 6, the periods obtained in this and referenced studies are compared with each other. When the periods obtained from SVEM are compared with SAP2000, it is seen that there is a good agreement between results. Moreover, results indicated that periods of isolated bridge with the TCFP bearing is longer than SCFP bearing.

In this study, quasi-static, dynamic and total components of internal forces and displacements of non-isolated and isolated bridge are investigated for different cases. The TCFP bearing devices used as seismic isolation are placed between deck and pier.

Means of maximum quasi-static, dynamic and total axial forces of the non-isolated and isolated bridge deck compared for Cases A to D are presented Fig. 13. The bridge supported on homogenous and inhomogeneous soil. The use of the TCFP bearing system may be reduced the maximum values of the quasi-static, dynamic and total axial forces of the bridge deck by 88%, 63% and 88%, respectively. These figures clearly indicated that while the smallest axial forces are obtained for the case B, the largest axial forces are obtained for the case C in both non-isolated and isolated bridge. Case A is more effective than Case D.

Means of maximum quasi-static, dynamic and total shear forces of the non-isolated and isolated bridge deck compared for cases A to D are presented Fig. 14. The bridge supported on homogenous and inhomogeneous soil. The use of the TCFP bearing system may be reduced the maximum values of the quasi-static, dynamic and total shear forces of the bridge deck by 93%, 61% and 88%, respectively. These figures clearly indicated that case C is more effective than other cases for the quasi-static, dynamic and total shear forces of the non-isolated bridge deck. While case A is more effective than other cases for dynamic and total shear forces, case C is more effective than other cases for quasi-static shear forces of isolated bridge deck.

Means of maximum quasi-static, dynamic and total bending moment of the non-isolated and isolated bridge deck compared for cases A to D are presented Fig. 15. The bridge supported on homogenous and inhomogeneous soil. The use of the TCFP bearing system may be reduced the maximum values of the quasi-static, dynamic and total bending moment forces of the bridge deck by 91%, 63% and 88%, respectively. These figures clearly indicated that case C is more effective than other cases for the quasi-static, dynamic and total bending moment of the non-isolated bridge deck. While case C is more effective than other cases for quasi-static and total bending moment, case A is more effective than other cases for dynamic bending moment of isolated bridge deck.

Means of maximum quasi-static, dynamic and total displacement of the non-isolated and isolated bridge deck compared for cases A to D are presented in Fig. 16. The quasi-static displacements of non-isolated and isolated bridge deck are very close together for case A-D. Means of maximum dynamic and total displacements of isolated bridge deck are bigger than those of non-isolated bridge by 284% and 61%, respectively. These figures clearly showed that while displacements in case of case C are the biggest for the quasi-static, dynamic and total displacements of the non-isolated and isolated bridge deck. The displacements in case of case B is the smallest. Also figures indicated that displacements in case of case A are bigger than those of case B.

7. Conclusions

In this paper, the stochastic response of the non-isolated and isolated bridge with the TCFP bearing system which is more effective than other sliding systems on severe earthquake ground motion is performed. The TCFP bearing system was designed and installed between bridge deck and pier. The incoherency, the wave passage and the site response effects are considered in the spatially varying ground motions. The analyses are carried out for non-isolated and isolated bridges, separately. The non-isolated and isolated bridge models subjected to spatially varying ground motions are compared their performance with each other. The means of maximum responses of the non-isolated and isolated bridges are also compared with each other for cases A to D. The results obtained from this study can be written as:

• The periods of the bridge isolated with the TCFP bearings longer than those of the isolated bridge with the SCFP and the DCFP bearings.

• The more difference between the local soil types at the support points, the more response values of isolated and non-isolated bridges occur. When the soil types come close to each other, values of internal forces decrease.

• The results obtained from the analyzes were compared with the help of graphs. It can be seen that the spatially varying earthquake motion is affected both for the isolated bridges and for the non-isolated bridge bridges.

• The use of isolation systems causes the bridge to be less affected during earthquakes.

• The use of the TCFP bearing system on the isolated bridge may be average reduced the total responses of the bridge deck by 85%.

• When the periods obtained from modal analyses in the SVEM and SAP2000 are compared, there is a good agreement between results.

• The response of the non-isolated bridge shows similar variance with those of the isolated bridge along the bridge deck length.

• In the isolated bridge, the modal mass participation ratio is as effective as the advanced modes than the non-isolated bridge.

References

Adanur, S., Altunisik, A.C., Soyluk, K., Bayraktar, A. and Dumanoglu, A.A. (2016), "Multiple-support seismic response of bosporus suspension bridge for various random vibration methods", *Case Stud. Struct. Eng.*, **5**, 54-67.

American Society of Civil Engineers-ASCE (2010), *Minimum Design Loads for Buildings and Other Structures*, Standard ASCE/SEI 7-10.

Apaydın, N.M., Bas, S. and Harmandar, E. (2016), "Response of the Fatih Sultan Mehmet suspension bridge under spatially varying multi-point earthquake excitations", *Soil Dyn. Earthq. Eng.*, **84**, 44-54.

Ates, S. and Constantinou, M.C. (2011), "Example of application of response spectrum analysis for seismically isolated curved bridges including soil-foundation effects", *Soil Dyn. Earthq. Eng.*, **31**(4), 648-661.

Ates, S. and Yurdakul, M. (2011), "Site-response effects on RC buildings isolated by triple concave friction pendulum bearings", *Comput. Concrete,* **8**(6), 693-715.

Ates, S., Bayraktar, A. and Dumanoglu, A.A. (2006), "The effect of spatially varying earthquake ground motions on the stochastic response of bridges isolated with friction pendulum systems", *Soil Dyn. Earthq. Eng.*, **26**(1), 31-44.

Ates, S., Dumanoglu, A.A. and Bayraktar, A. (2005), "Stochastic response of seismically isolated highway bridges with friction pendulum systems to spatially varying earthquake ground motions", *Eng. Struct.*, **27**(13), 1843-1858.

Ates, S., Soyluk, K., Dumanoglu, A.A. and Bayraktar, A. (2009), "Earthquake response of isolated cable-stayed bridges under spatially varying ground motions", *Struct. Eng. Mech.*, **31**(6), 639-662.

Barbas, J., Matusewitch, P. and Williams, M. (2011), "Comparative of single pendulum and triple pendulum seismic isolation bearings on the St. Laurent Bridge, Quebec, Canada", *Proceedings of the 6th New York City Bridge Conference on Modern Techniques in Design, Inspection, Monitoring and Rehabilitation of Bridge Structures,* New York, U.S.A., July.

Bucher, C. (2011), "Optimal friction pendulum systems for seismic isolation", *Proceedings of the 8th International Conference on Structural Dynamics*, Leuven, Belgium, July.

Button, M.R., Der Kiureghian, A. and Wilson, E.L. (1981), *STOCAL-User Information Manual, Report No UCB/SEMM-81/2,* Department of Civil Engineering, University of California, Berkeley, California, U.S.A.

Clough, R.W. and Penzien, J. (1993), *Dynamics of Structures,* 2nd Edition, McGraw Hill, Inc., Singapore.

Computers and Structures Inc (2007), *SAP2000: Static and Dynamic Finite Element Analysis of Structures*, Berkeley, California, U.S.A.

Constantinou, M.C., Kalpakidis, I., Filiatrault A. and Ecker Lay, R.A. (2011), *LRFD-Based Analysis and Design Procedures for Bridge,* Technical Report.

Der Kiureghian, A. and Neuenhofer, A. (1991), *A Response Spectrum Method for Multiple-Support Seismic Excitations, Report No. UCB/EERC-91/08,* Earthquake Engineering Research Center, College of Engineering, University of California, Berkeley, California, U.S.A.

Der Kiureghian, A. (1980), "Structural response to stationary excitation", *J. Eng. Mech. Div.*, **106**(6), 1195-1213.

Dumanoglu, A.A. and Severn, R.T. (1987), "Seismic response of modern suspension bridges to asynchronous vertical ground motion", *Inst. Civil Eng. Proc.*, **2**(83), 701-730.

Dumanoglu, A.A. and Severn, R.T. (1990), "Stochastic response of suspension bridges to earthquake forces", *Earthq. Eng. Struct. Dyn.*, **19**(1), 133-152.

Dumanoglu, A.A. and Soyluk, K. (2002), *SVEM, A Stochastic Structural Analysis Program for Spatially Varying Earthquake Motinos*, Turkish Earthquake Foundation, TDV/KT 023-76, Istanbul, Turkey.

Fadi, F. and Constantinou, M.C. (2009), "Evaluation of simplified methods of analysis for structures with triple friction pendulum isolators", *Earthq. Eng. Struct. Dyn.*, **39**(1), 5-22.

Fallahian, M., Khoshnoudian, F. and Loghman, V. (2015), "Torsionally seismic behavior of triple concave friction pendulum bearing", *Adv. Struct. Eng.*, **18**(12), 2151-2166.

Fenz, D.M. and Constantınou, M.C. (2008a), "Spherical sliding isolation bearings with adaptive behavior: Theory", *Earthq. Eng. Struct. Dyn.*, **37**(2), 163-183.

Fenz, D.M. and Ve Constantinou, M.C. (2008b), "Modeling triple friction pendulum bearings for response history analysis", *Earthq. Spectr.*, **24**(4), 1011-1028.

Harichandran, R.S. and Vanmarcke, E.H., (1986), "Stochastic variation of earthquake ground motion in space and time", *J. Eng. Mech.*, **112**(2), 154-174.

Harichandran, R.S. and Wang, W. (1988), *Response of One-and Two-Span Beams to Spatially Varying Seismic Excitation*, Report to the National Science Foundation MSU-ENGR-88-002, Department of Civil and Environmental Engineering, College of Engineering, Michigan State University, Michigan, U.S.A.

Harichandran, R.S., Hawwari A. and Sweidan B.N. (1996), "Response of long-span bridges to spatially varying ground motion", *J. Struct. Eng.*, **122**(5), 476-484.

Loghman, V. and Khoshnoudian, F. (2015), "Comparison of seismic behavior of long period SDOF systems mounted on friction isolators under near-field earthquakes", *Smart Struct. Syst.*, **16**(4), 701-723.

Lou, L. and Zerva, A. (2005), "Effects of spatially variable ground motions on the seismic response of a skewed, multi-span, RC highway bridge", *Soil Dyn. Earthq. Eng.*, **25**(7), 729-740.

Morgan, T.A. and Mahin, S.A. (2012), "Achieving reliable seismic performance enhancement using multi-stage friction pendulum isolators", *Earthq. Eng. Struct. Dyn.*, **41**(3), 355-373.

Nakamura, Y., Der Kiureghian, A. and Liu D. (1993), *Multiple-Support Response Spectrum Analysis of the Golden Gate Bridge*, Report No. UCB/EERC-93/05, Earthquake Engineering Research Center, College of Engineering, University of California, Berkeley, California, U.S.A.

Priestley, M.J.N., Seible, S. and Calvi, G.M. (1996), *Seismic Design and Retrofit of Bridges*, John Wiley and Sons, 184, 242.

Scheller, J. and Constantinou, M.C. (1999), *Response History Analysis of Structures with Seismic Isolation and Energy Dissipation Systems: Verification Examples for SAP2000*, Technical Report MCEER-99-0002, Buffalo, U.S.A.

Soyluk, K. and Dumanoglu, A.A. (2004), "Spatial variability effects of ground motions on cable-stayed bridges", *Soil Dyn. Earthq. Eng.*, **24**, 241-250.

Tajammolian, H., Khoshnoudian, F., Talaei, S. and Loghman, V. (2014), "The effects of peak ground velocity of near-field ground motions on the seismic responses of base-isolated structures mounted on friction bearings", *Earthq. Struct.*, **7**(6), 1259-1281.

Wang, H., Li., J., Tao1, T., Wang, C. and Li, A. (2015), "Influence of apparent wave velocity on seismic performance of a super-long span triple-tower suspension bridge", *Adv. Mech. Eng.*, **7**(6), 1-14.

Yurdakul, M. and Ates, S. (2011), "Modeling of triple concave friction pendulum bearings for seismic isolation of buildings" *Struct. Eng. Mech.*, **40**(3), 315-334.

Yurdakul, M., Ates, S. and Altunisik, A.C. (2014), "Comparison of the dynamic responses of Gulburnu highway bridge using single and triple concave friction pendulums", *Earthq. Struct.*, **7**(4), 511-525.

Zayas, V.A., Low, S.S., Mahin, S.A. and Bozzo, L. (1989), *Feasibility and Performance Studies on Improving the Earthquake Resistance of New Existing Building Using the Friction Pendulum System*, Report No. UCB/EERC 89-09, Earthquake Engineering and Research Center, College of Engineering, University of California, Berkeley, California, U.S.A.

Zerva, A. (1991), "Effect of spatial variability and propagation of seismic ground motions on the response of multiply supported structures", *Probabilst. Eng. Mech.*, **6**(3-4), 212-221.

CC